Determination of the J integral for laminated double cantilever beam specimens: The curvature approach

Rask, Morten; Sørensen, Bent F.

Published in:
Engineering Fracture Mechanics

Link to article, DOI:
10.1016/j.engfracmech.2012.06.017

Publication date:
2012

Determination of the J integral for laminated double cantilever beam specimens: The curvature approach

M. Rask[a,*], B.F. Sørensen[a]

[a]*DTU Wind Energy, Risø Campus, Technical University of Denmark, 4000 Roskilde, Denmark*

Abstract

A new approach is proposed for measuring the J integral (and thus the fracture resistance) of interface cracks in multiply laminates. With this approach the J integral is found from beam curvatures and applied moments. Knowledge of ply layup and stiffness is not required. In order to test the accuracy of the proposed approach, double cantilever beam specimen loaded with uneven bending moments (DCB-UBM) specimens were tested and analysed using the curvature approach and a method based on laminate beam theory. Beam curvatures were determined using a configuration of strain gauges. Good agreement was obtained between the two approaches.

Keywords: Fibre reinforced materials, Bridging, Delamination, Interface fracture, J integral

1. Introduction

The rotor blades of modern wind turbines are made primarily of composite laminates and sandwich structures [1]. A type of failure often seen in laminates and sandwich structures is delamination, e.g. cracking along interfaces between plies, along adhesive/laminate interfaces and along sandwich/core interfaces.

There is an increasing interest in the use of cohesive zone modelling in the simulation of delamination of components. In cohesive zone modeling, the fundamental constitutive law that describes the mechanics of the fracture process is a traction-separation law called a cohesive law. Several commercially available finite element programs have capabilities for simulations using cohesive zone modelling. However, the determination of cohesive law parameters remains an important experimental challenge.

Most approaches for experimental determination of cohesive laws involve numerical simulations of a test specimen loaded to failure. The fracture plane is modelled by a cohesive zone and the cohesive law is determined indirectly by iteratively guessing and comparison of measured and predicted overall response, e.g. load-displacement relations [2, 3, 4]. A more direct approach - one that does not require modelling of the test specimen with a cohesive zone - is to derive the cohesive law by differentiation of the J integral by the end-opening of the fracture process zone [5, 6, 7]. This approach has recently been extended to determination of mixed-mode cohesive laws [8, 9].

The J integral is particularly useful in the analysis of beam-type specimens that exhibit a large-scale bridging zone [10, 7]. A remarkable J integral analysis is that of a Double Cantilever Beam (DCB) specimen loaded with wedge forces [6, 11]. For this specimen configuration, the J integral result for each arm is simply the product of the instantaneous values of the applied force per unit width and the beam rotation at the loading point. The prior load-displacement history, the specimen thickness and the elastic (linear and non-linear) properties of the beams are not required [6, 11]. This analysis is valid also for large-scale bridging zones. This specimen configuration has been used for the deduction of the cohesive laws of adhesive joints using the approach involving J and the end-opening, as described above [12, 13].

*Corresponding author
Email addresses: mrask@dtu.dk (M. Rask), bsqr@dtu.dk (B.F. Sørensen)

The analysis of laminates and multilayers consisting of elastic materials (assuming small-scale yielding) can also be analysed by evaluating the J integral around the external boundaries. For DCB specimens loaded with axial forces and/or bending moments, the J integral can be expressed in terms of the instantaneous values of the applied forces and moments. However, for laminates consisting of many layers (lamina), the calculations are involving and may best be handled numerically, e.g. using an analysis based on laminate theory [14, 15, 16]. A drawback of this approach is that the thickness and elastic properties of each layer must be known; this is particularly challenging for laminates with significant amount of off-axis plies for which the elastic properties may not be accurately known. An approach based on gluing thick and stiff skins with known elastic properties to the specimens can be used for reducing the sensitivity of elastic properties of thin layers [16].

The study of large-scale bridging and large-scale active cohesive zones involves special considerations. In general, J integral solutions differ from potential energy release rate solutions based on linear-elastic fracture mechanics analysis of stress intensity factors [10]. Exceptions are beam-type specimens loaded with axial forces and moments [7]. As such, a DCB specimen loaded with Uneven Bending Moments (DCB-UBM) was recently proposed for characterization of mixed-mode crack growth in composites exhibiting large-scale bridging [17]. For specimens consisting of elastic beams, the J integral can be determined in closed analytical form and the only experimental data required is the instantaneous value of the applied moments (along with specimen dimensions and elastic properties); no measurement of beam rotation or crack length is required. For this test configuration, the J integral result is independent of crack length, giving stable crack growth under any mode I - mode II combination.

1.1. Problem statement

In this paper, we propose an approach for the determination of the J integral for the DCB-UBM test specimen from the instantaneous values of the applied moments and the beam curvatures. The analysis remains valid for large-scale bridging problems as long as the beams behave linear-elastically. No knowledge is required of the thickness and elastic properties of the individual layers. Therefore, the method is particularly suited for the analysis of large-scale bridging problems of laminates consisting of many layers having different elastic properties. As such, the present study answers the question raised by Paris and Paris [11] whether other specimen configurations can be found for which the J calculation are equally direct as the DCB loaded with wedge forces.

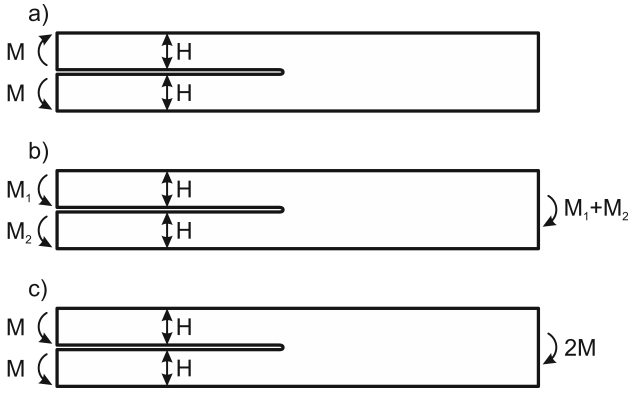

Figure 1: The homogeneous Double Cantilever Beam loaded with Uneven Bending Moments (DCB-UBM) specimen under different load combinations; a) a nominal mode I load, b) a mixed mode load and c) a nominal mode II load.

As mentioned, the DCB-UBM test configuration is loaded by a combination of bending moments, as shown in Fig. 1. A nominal mode I loading is shown in Fig. 1a. With moments defined positive downwards as shown in Fig. 1b, the nominal mode I load state occurs when $M_1 = -M_2$. In Fig. 1b, a mixed mode loading is shown. Then, the moments applied to the beam fulfills $M_1 \neq |M_2|$. In Fig. 1c, a nominal mode

II loading is seen ($M_1 = M_2$). By varying the relations between M_1 and M_2 any mode combinations can be attained.

In this study we develop the curvature model, based on Bernoulli beam theory, and test the proposed approach using adhesive joint specimens, i.e. laminate beams joined by an adhesive layer. The methodology is valid also for specimens made of dissimilar beams. The cracking will occur along one of the adhesive/beam interfaces, meaning that the DCB specimens were not fully symmetric. Therefore, the crack growth is always mixed mode, and the terms *nominal* mode I and mixed mode is used in the remainder of this text.

2. Theory

2.1. The curvature model

The J integral is valid for small strains, rotations and displacements. Generally, the J integral is defined as [18, 19]:

$$J = \int_\Gamma \left[\Phi dx_2 - \sigma_{ij} n_j \frac{\partial u_i}{\partial x_1} dS \right] \tag{1}$$

where Φ is the strain energy density, σ_{ij} is the stress tensor, u_i is the displacement vector, n_j is the outwards unit vector normal to the integration path Γ and S denotes the length of the path Γ. The J integral is path independent [19], implying that J takes the same value for any integration path that goes around the fracture process zone from the lower crack face to the upper crack face in the counter clockwise direction, as indicated with the dotted line in Fig. 2. As the beams are loaded with pure moments, the shear stresses

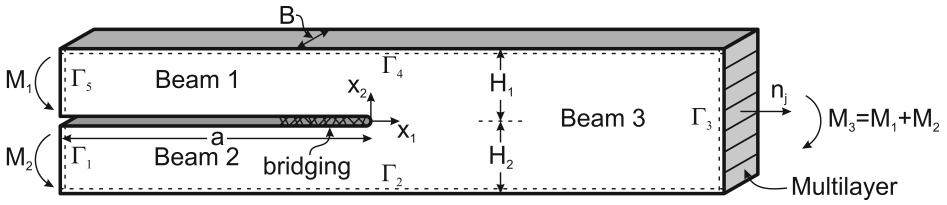

Figure 2: Generic DCB-UBM specimen with a large-scale bridging zone. The counter-clockwise integration path is shown.

along the boundaries vanish away from the crack tip and bridging zone, i.e. $\sigma_{ij} \to 0$ for $i \neq j$ and both σ_{ij} and the strain tensor ε_{ij} are independent of x_1 away from the fracture process zone, where the beams are subjected to pure bending. Then, for linearly elastic materials, the strain energy density is

$$\Phi = \frac{1}{2} \sigma_{11} \varepsilon_{11}. \tag{2}$$

We now examine the integration path Γ_1 illustrated in Fig. 2. With $n_j = (-1, 0, 0)$ the second term in Eq. (1) can be rewritten using

$$\sigma_{ij} n_j \frac{\partial u_i}{\partial x_1} = \sigma_{11} n_1 \frac{\partial u_1}{\partial x_1} = -\sigma_{11} \varepsilon_{11}. \tag{3}$$

Since the x_1-components of displacement and strain relate by

$$\frac{\partial u_1}{\partial x_1} = \varepsilon_{11} \tag{4}$$

eqs. (2) and (3) are the J integral-contribution along the integration path Γ_1. With $dS = -dx_2$ at $x_1 = -a$, the J integral contribution along Γ_1 ($x_1 = -a$ and $-H_2 \leq x_2 \leq 0$) becomes

$$J_1 = -\int_0^{-H_2} \frac{\sigma_{11}(x_2)\varepsilon_{11}(x_2)}{2} dx_2. \tag{5}$$

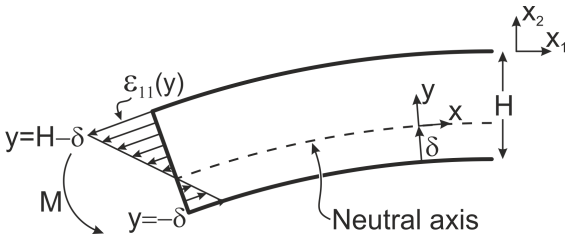

Figure 3: Moment and curvature and defined positive downwards. The strain distribution across the beam, resulting from a pure moment is indicated.

This expression is valid for plane stress as well as plane strain. Note that in a multi-layer, the stress σ_{11} is, unlike the strain ε_{11}, discontinous from layer to layer, and in a laminate based analysis [16] the integration paths would be subdivided into one path per layer.

In the following, it is convinient to use multiple coordinate systems - a global x_1, x_2-system with origo at the crack tip, and a local x, y-system for each beam with origo at the neutral axis of each beam positioned a distance δ from the bottom of the beam. Both systems are defined in Fig. 3, where a positive bending moment and curvature is shown. The neutral axis is shown as a dotted line at $y = 0$ with $y = x_2 + H - \delta$. For a symmetric beam, the neutral axis coincides with the geometrical midplane, $\delta = H/2$.

Changing Eq. (5) from the x_1, x_2 system to the x, y system we get

$$J_1 = -\int_{H_2-\delta}^{-\delta} \frac{\sigma_{11}(y)\varepsilon_{11}(y)}{2} dy. \tag{6}$$

Under the assumptions of small rotations and displacements, the strain profile along the y-axis for a multi-layered beam subjected to bending is linear, as indicated in Fig. 3.

$$\varepsilon_{11}(y) = \kappa^0 y \tag{7}$$

where κ^0 denotes the curvature of the neutral axis. Still examining integration path Γ_1 Eqs. (6) and (7) are combined to give

$$J_1 = -\frac{\kappa_1^0}{2}\int_{H_2-\delta}^{-\delta} \sigma_{11}(y) y dy = \frac{\kappa_1^0}{2} \cdot \frac{M_2}{B}$$

with B denoting the width of the specimen and the moment is defined by

$$M_2 = B\int_{-\delta}^{H_2-\delta} \sigma_{11}(y) y dy. \tag{8}$$

Similar results can be obtained for the other beam ends. There are no contributions to the J integral from integration paths Γ_2 and Γ_4 where $dx_2 = 0$ and $\sigma_{ij} n_j = 0$. Thus, the total J integral can be found by summing the three beam-end contributions, i.e. along Γ_1, Γ_3 and Γ_5. The result is

$$J = \frac{\kappa_1^0}{2} \cdot \frac{M_1}{B} + \frac{\kappa_2^0}{2} \cdot \frac{M_2}{B} - \frac{\kappa_3^0}{2} \cdot \frac{M_1 + M_2}{B} \tag{9}$$

where κ_2^0 and κ_3^0 are the curvatures at the neutral axes of beams 2 and 3 respectively. The third term is negative in agreement with the direction of the integration path Γ_3.

The result Eq. (9) shows that we can determine the J integral by measuring the applied moment and the curvature of the neutral axis for each beam. Note, that the elastic properties (or layup sequence, anisotropy etc.) of the beams of the DCB specimen are not required. This implies that for a complex multilayered DCB specimen, even with unknown materials and unknown layup sequence, the J integral can obtained by measuring the curvature of the beams, the applied moments and the width of the beams.

The proposed *curvature approach* was verified analytically against known results from the literature. The verification examples were a bi-layer specimen [16], sandwich specimens with center or interface cracks [9, 20] and five-ply laminate [16]. In all cases, complete analytical agreement was found between the curvature model and the results from the literature.

2.2. Curvatures from strains

It can fairly easily be shown that the curvature of the neutral axis of a beam κ^0 can be found from the normal strain ε_{11} at the top and bottom of the beam. This is beneficial since, if we know the strains in the top and bottom, the curvature can be calculated, without knowledge of the position of the neutral axis. It follows from Eq. (7) that the strain in the top and bottom of the beam can be obtained as

$$\varepsilon_{11}^t = \kappa^0(H - \delta) \quad \text{and} \quad \varepsilon_{11}^b = -\kappa^0\delta. \tag{10}$$

with H denoting the height of the beam in question, and superscripts t and b denoting respectively the top and bottom of the beam in a global system of reference. δ is eliminated to arrive at

$$\kappa^0 = \frac{\varepsilon_{11}^t - \varepsilon_{11}^b}{H}. \tag{11}$$

For instance for the top beam, beam no. 1, in Fig. 2 the curvature of the beam can be expressed as

$$\kappa_1^0 = \frac{\varepsilon_{11}(y = H_1 - \delta) - \varepsilon_{11}(y = -\delta)}{H_1}. \tag{12}$$

In the derivation of Eq. (11) it was assumed that the beams experience pure bending. This means that no matter which method (strain gauges, optical methods, etc.) is chosen for determining the necessary strains, it must be done in a region of the beam free of effects from the beam end and the fracture process zone (crack tip and bridging zone) in correspondence with *de Saint-Venant's principle*.

If the beam in question is symmetric such that the neutral axis lies in the midplane of the beam ($\delta = H/2$), the strains will be opposite and numerically equal at the top and bottom of the beam, i.e. $\varepsilon_{11}^t = -\varepsilon_{11}^b$. Then it is only necessary to determine the strain at either the top or bottom surface of each beam. For instance, if the strain is determined on the top of the beam, the curvature can be calculated as

$$\kappa_{sym}^0 = \frac{2\varepsilon_{11}^t}{H} \tag{13}$$

where the subscript *sym* indicates that Eq. (13) is only valid for symmetric beams.

3. Experimental evaluation of the curvature approach

3.1. Overall idea

In order to validate the curvature approach, a test programme was set up in which a number of specimens were tested, and the data were analysed using both the laminate theory approach of Lundsgaard-Larsen et al [16] and the curvature approach to extract the J integral values. This enables direct comparison of the two approaches. The DCB test specimens were made from two glass fibre/polyester composite beams joined by an adhesive layer. The beams had two different layups giving different stiffnesses. The layups consisted of two different lamina denoted material A and material B, with material A being less stiff than material B. However, the material/adhesive interface to be tested was the same in all samples. The samples were subjected to two different load configurations. The load configurations were chosen to minimize the number of required strain gauges. The first was a nominal mode I configuration with $M_1 = -M_2$ and $M_3 = 0$. With this configuration, the uncracked end will have zero loading and thus zero curvature. The second was a mixed mode load configuration with $M_1 = 0$ and $M_2 = M_3$. Beam 1 will have zero loading and thus zero curvature. This means that in both cases, only two of the three beam ends would have non-zero curvature,

Parameter	Variants	Comments
Materials	A and B	Material B is stiffer than material A
Layups	1 and 2	Layup 1 is stiffer than layup 2
Load configurations	Nominal mode I	$M_1 = -M$, $M_2 = M$ and $M_3 = 0$
	Mixed mode	$M_1 = 0$, $M_2 = M$ and $M_3 = M$
Analysis methods	Curvature approach	Beam curvatures from strain gauges
	Laminate theory approach	Lamina thicknesses and stiffnesses must be measured

Table 1: Overview of the test programme.

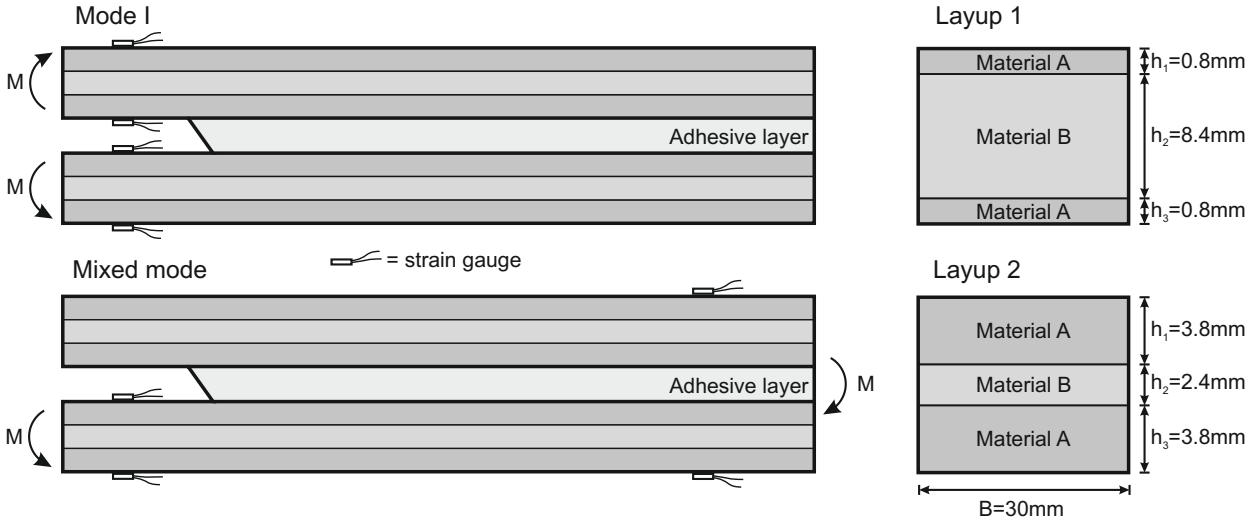

Figure 4: Left: DCB specimens made by joining two symmetric 3-ply beams (thickness 10 mm) with an adhesive layer (thickness 5 mm). The two load configurations are illustrated. The mode I load configuration corresponds to $M_1 = -M$, $M_2 = M$ and $M_3 = 0$, while the mixed mode configuration corresponds to $M_1 = 0$, $M_2 = M$ and $M_3 = M$. The locations of the strain gauges are illustrated. Right: Sketches of the two layups.

so that only two of the three beam ends would need to be fitted with strain gauges, see Fig. 4. An overview of the test programme is shown in Table 1.

Laminates consisting of six layers joined by an adhesive were used, see Fig. 4. The layups were made from combinations of two different glass fibre/polyester composite materials, see Section 3.2.1. For reasons of confidentiality these are referred to simply as material A and material B. Material B is approximately three times as stiff as material A, due to a large amount of 0°-fibres, whereas material A mainly contains off-axis fibres.

Two different types of specimens with different layups were made. In layup 1, the central layer of material B has a nominal thickness of 8.4 mm, while the central layer in layup 2 has a nominal thickness of 2.4 mm. All beams had nominal thicknesses of 10 mm. This means that layup 1 contains a higher ratio of the stiffer material B, whereby layup 1 is expected to be stiffer than layup 2. However, since fracture occurs along similar material interfaces for the two specimen types, similar J integral curves are expected for the two layups.

The test programme included twelve specimens, divided in four groups of three: L1MI, L1MM, L2MI and L2MM, with L1 and L2 denoting layup 1 and layup 2 while MI and MM denotes nominal mode I and mixed mode, respectively. The thickness of all seven layers (six composite plies and the adhesive layer) of each specimen are needed for the analysis based on the laminate beam theory approach. Thus, the thickness of each of these layers were measured at three positions along the specimen, and the average of each set of

three measurements were entered in a database.

3.2. Experimental work

3.2.1. Specimen manufacturing

The laminates for the test specimens were supplied by Danish manufacturer of wind turbine blades LM Wind Power A/S. The DCB specimens were manufactured as follows. First, a laminate panel (600 by 600 mm, thickness approximately 10 mm) of each glass fibre/polyester layup were made by the techniques of hand layup and matrix impregnation by vacuum infusion. After consolidation, 15 beams (length 500 mm, width 30 mm) were cut from each panel. To make six DCB specimens of each layup, the beams were bonded together in pairs with a thermoset adhesive (Oldopal 0555 VE from Büfa, hardened at 40°C for 16h). A slip foil (thickness 12.7 μm) was placed at the one end of the beams to define a sharp crack initiation location. Spacers (5 mm) were used to control the thickness of the adhesive layer. Steel grips were fixed to each beam with four steel screws and an epoxy adhesive (Scotch-Weld DP 460 from 3M, hardened at 40°C for 2h). Holes (diameter 1.5 mm) were drilled at the end of the slip foil (where crack growth will start) and steel pins were inserted. These were to be used for mounting of extensometers. Finally, strain gauges (0°, gauge length 10 mm) were fixed to the beams to be subjected to bending according to Fig. 4. In accordance with de Saint-Venant's principle, strain gauges were placed a distance of two times the beam height away from the gripping fixtures on the specimens. Fig. 5 shows a detailed drawing of a finished specimen.

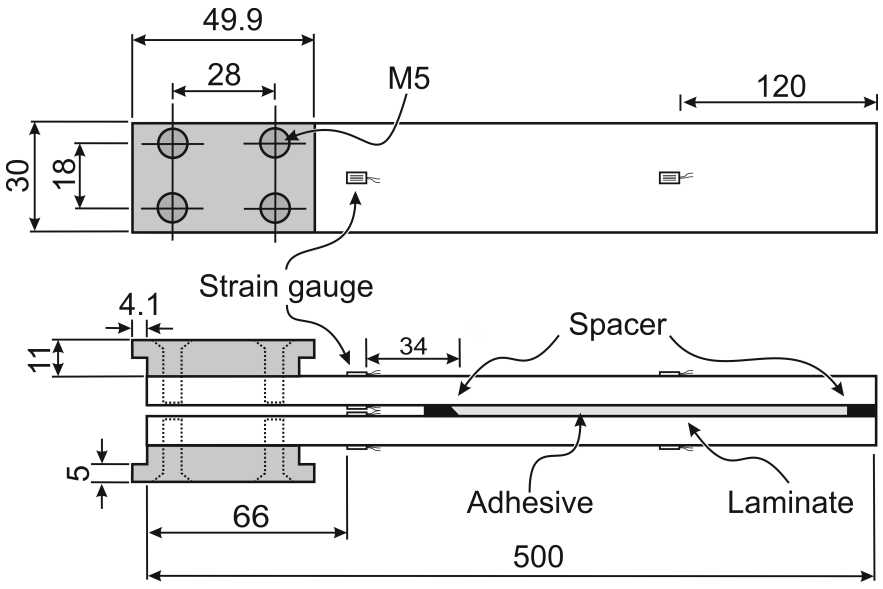

Figure 5: Drawing of specimen. Positions for both mode I and mixed mode tests are shown.

3.2.2. Measurement of elastic properties

Spare beams, not used for manufacturing DCB specimens, were subjected to tensile tests on a standard servo-hydraulic test machine fitted with a 100 kN load cell (Instron UK1029). Three beams of each layup were tested to strains of 0.3%. Strains were determined with a extensometer (Instron 1562, gauge length 50 mm). The tests were run at a displacement rate of 0.01 mm/s. Readings from the extensometer and load cell were collected at a PC at 10Hz. The stiffness for each layup were found by making linear regression to the stress-strain data in the strain interval 0.05-0.25%. From these values, the Young's moduli of the two materials A and B were determined. By performing tensile tests of both layups, the effective stiffness $\bar{E}$ of each layup was determined. Then, the rule of mixtures could be employed to back-calculate the effective stiffness values of the materials A and B.

Note that knowledge of the Young's moduli of the two materials is not required for the curvature approach (Eq. 9), but is a required input in an analysis based on laminate theory, see section 3.3.2.

3.2.3. DCB test method

The DCB-UBM specimens were tested on a special test device, shown schematically in Fig. 6. The testing fixture and procedure is described in detail in [17]. With two load cells and an arrangement of wires and

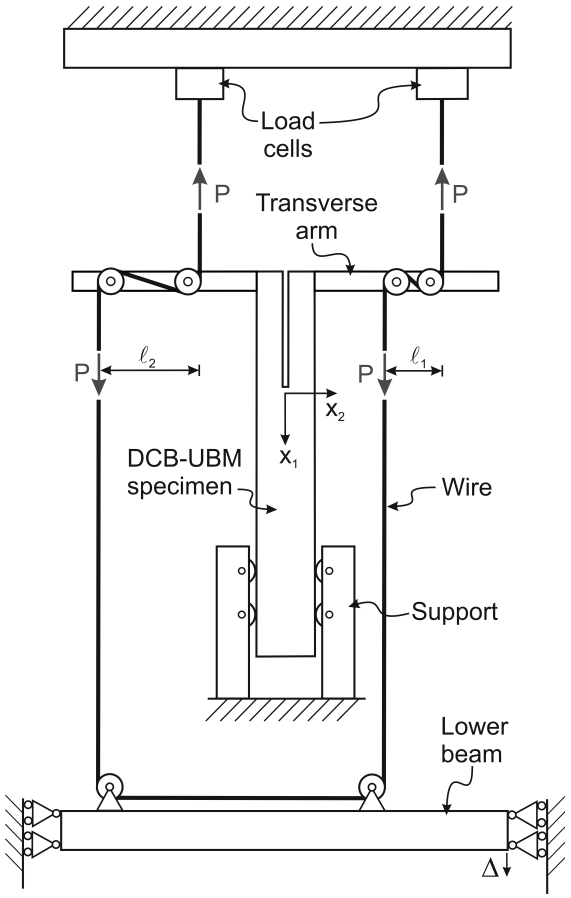

Figure 6: A schematic drawing of the testing device. Adapted from [9].

rollers, the test fixture allows for the test specimen to be tested under any combination of bending moments. The wires apply the same force to two rollers located at each of the transverse arms mounted on each beam of the DCB specimen, creating pure bending moments. As moment = force × arm, a configuration with different moment arms on each side gives different moments on the two beams, even though the forces P are of identical magnitude at both transverse arms. Adjusting the device from one load configuration to another is simply a matter of altering the lengths of the moments arms by changing the position of the rollers on the transverse arms. The moments are written as

$$M_1 = P\ell_1, M_2 = P\ell_2. \tag{14}$$

By adjusting ℓ_1 and keeping ℓ_2 fixed any moment combination can be obtained. The wire force is increased by moving the lower part of the test device (denoted *lower beam* in Fig. 6) downwards at a constant displacement rate.

The test was conducted as follows. First, a DCB specimen was mounted at the test device. The transverse arms and the wire was mounted. Next, an extensometer (Instron type 2620–601, range ±5 mm),

was mounted at the steel pins to record the end-opening. The strain gauges were connected to a strain gauge amplifier (HBM MGCplus AB22A). The displacement rate of the lower beam was 10 mm/min. Pictures were taken during the experiments, and data for the two load cell readings (N), the extensometer opening (mm) and the four strain gauge readings (%) were logged at 25Hz.

3.3. Data analyses

The datasets for each specimen were analysed using both the curvature approach and the laminate beam theory approach, whereby the outcome of the two approaches can be compared. In both cases, the adhesive layer is ignored. This is a reasonable approximation, as the adhesive is much softer than the glass fibre beams.

3.3.1. Curvature approach

From the loads and the length of the moment arms, ℓ_1 and ℓ_2, the moments were calculated for each data point using Eq. (14). The curvature at each data point were determined from the strain gauge data using Eq. (11). From the moment and curvature values, the J integral was calculated for each beam and the total J integral value was obtained as the sum of the contributions from each beam, according to Eq. (9).

3.3.2. Laminate beam theory approach

For the laminate beam theory data analysis, a Matlab code acquired from [16] was modified so that the J integral was calculated for each data point. The J integral was determined using the result from [16]

$$J = \sum_{p=1}^{\tilde{p}} \frac{E_p M_b^2}{6\left(D_b A_b - B_b^2\right)^2} \left[A_b^2\left(y_{p-1}^3 - y_p^3\right) - 3A_b B_b\left(y_{p-1}^2 - y_p^2\right) + 3B_b^2\left(y_{p-1} - y_p\right)\right] \tag{15}$$

where $p = 1, 2, \ldots, \tilde{p}$ is the integration path number indicated in Fig. 2, $b = 1, 2, 3$ is the beam index, E_p is the Young's modulus of the ply related to integration path p and y_p is the lower (in the global system) interface of that ply. A_b, B_b and D_b are the extension, coupling and bending terms for beam b. For the sake of brevity, the definitions of these terms are not given here; they can be found in [16].

4. Results

4.1. Material stiffnesses

Table 2 lists the effective Young's modulus $\bar{E}$ in the x_1-direction for the two materials used to make the layups. The term *effective* is used to point out that these stiffness values are found experimentally as the values when the materials are fixed in the described layups, i.e. not from tests of the individual layers alone.

Material	$\bar{E}$ (GPa)
A	14.6 ± 0.09
B	49.1 ± 1.4

Table 2: Effective Young's modulus with standard deviation for the two materials.

4.2. Overview of failure modes of DCB-UBM specimens

Crack growth initiated from the slip foil along the adhesive/laminate interface. It was, however, observed that the four groups of specimens developed different damage mechanisms. As shown in Fig. 7a-b, the mode I test specimens (groups L1MI and L2MI) cracked along a single crack path at the material/adhesive interface with the formation of large-scale bridging by glass fibres. Layup 1 tested in mixed mode (L1MM), Fig. 7c, cracked in two planes with one fracture plane at the adhesive/material A interface and a second plane at the material A/material B interface. Layup 2 tested in mixed mode (L2MM), Fig. 7d, cracked in three planes with one plane at the adhesive/material A interface and two planes in the material A ply.

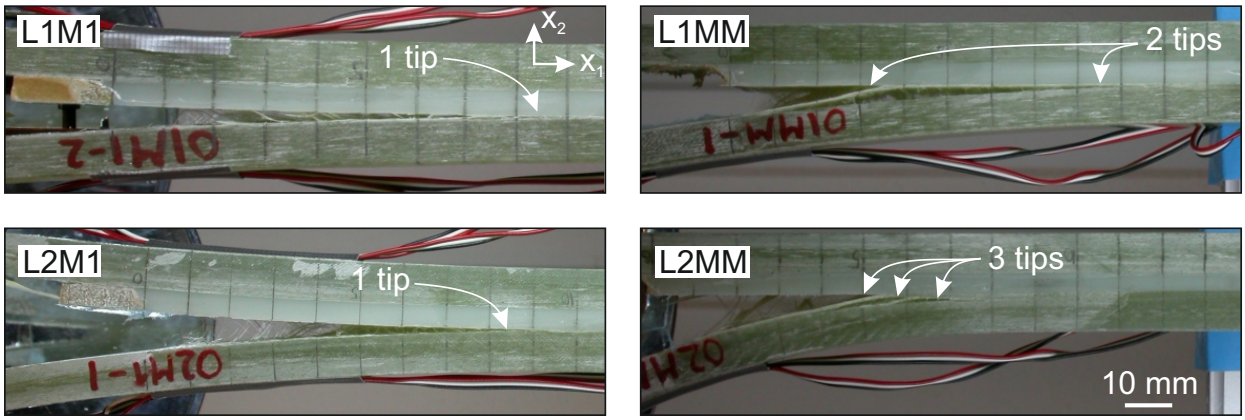

Figure 7: Photographs of four test specimens during crack growth. The pictures show a characteristic specimen from each of the four test groups a) L1MI, b) L2MI, c) L1MM and d) L2MM.

4.3. Fracture resistance data

J integral results from the two approaches are plotted as a function of the end-opening δ^* for mode I experiments and mixed mode experiments in Figs. 8 and 9 respectively. The data plots in Figs. 8 and 9

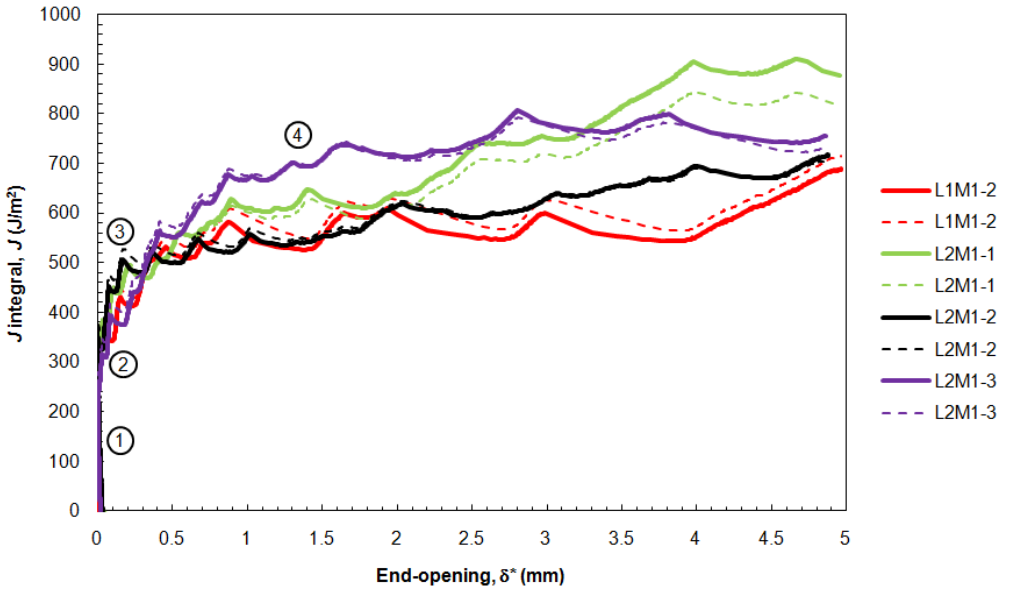

Figure 8: J integral as a function of end-opening δ^* for specimens tested in nominal mode I configuration. The solids lines show results from the curvature model, while the dotted lines show results from the laminate theory model. The specimens L1MI-1 and L1MI-3 are not included since the crack kinked into the adhesive layer right after crack initiation for these specimens.

all have the same characteristic appearance which can be described in four phases (phases indicated in Fig. 8): In phase 1, the J integral value increases without causing crack growth. Then, in phase 2 crack growth initiates. In phase 3, the J integral value increases rapidly with a continuous increase in δ^*. During this phase, the crack tip advances and a fracture process zone of bridging fibres develops. At an end-opening of roughly 1 mm (phase 4) the J integral increases more slowly and almost linearly with δ^*, approaching a steady state value. During the tests, a significant amount of fibre bridging was seen, see Fig. 7. Fibre bridging is known to increase the fracture resistance [21].

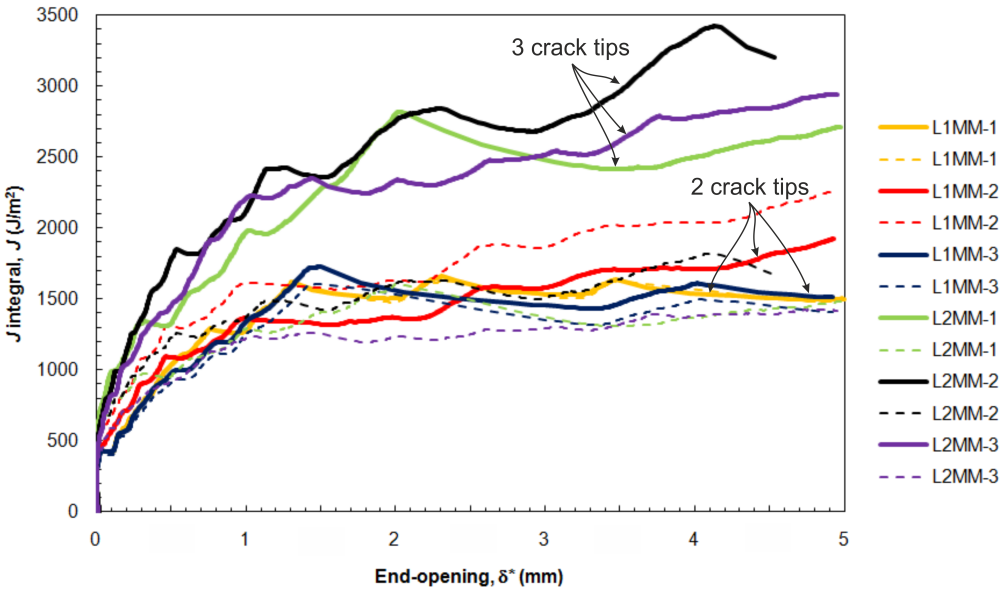

Figure 9: J integral as a function of end-opening δ^* for specimens tested in mixed mode configuration. For the curvature model curves (solid lines) it has been indicated whether the crack front had two or three crack tips.

The crack growth initiation values J_0 for all samples are listed in Table 3. Crack initiation was defined as an end-opening of 20 μm. The average values with standard deviations are $314 \pm 49 J/m^2$ and $392 \pm 60 J/m^2$ for the mode I tests and the mixed mode tests, respectively.

Specimen	J_0 (J/m^2)	Specimen	J_0 (J/m^2)
L1MI-1	-	L1MM-1	437
L1MI-2	358	L1MM-2	319
L1MI-3	-	L1MM-3	320
L2MI-1	320	L2MM-1	425
L2MI-2	333	L2MM-2	460
L2MI-3	245	L2MM-3	390

Table 3: Values of fracture resistance for crack growth initiation along the laminate/adhesive interface. Values are taken from the curvature approach analyses. Values from specimens L1MI-1 and -3 have been omitted as the crack in these specimens initiated in the adhesive layer.

The results from the nominal mode I tests in Fig. 8 show that the two approaches gives J, δ^*-curves with roughly the same shape and deviations of $0 - 10\%$.

Fig. 9 shows the results from mixed mode tests of the two approaches. Again, the J, δ^*-curves follow the same pattern for the two approaches. L1MM-1 shows deviations of about 1%. For L1MM-2, the laminate theory approach gives J values about 15% larger the the curvature approach, and for L1MM-3, the curvature approach gives J values about 6% larger than the laminate theory approach. The layup 2 experiments shows curves of similar appearances for the two approaches. However, the deviations are very large: The curvature approach gives J integral values about 83-102% higher than the laminate theory approach.

The large deviations for the L2MM group was investigated by studying the beam curvatures: From the pictures taken during the experiments, the actual curvatures of the beams were determined by fitting circles to the photographs of the bent beams. With the laminate theory formulation, the beam curvatures were calculated from the geometry, layup configuration, stiffness and thickness of each ply and applied moments. Thereby, it was found that the predictions of beam curvature from the curvature approach and

the laminate theory approach were respectively 1-5% and 47-51% below the actual curvature determined from the photographs.

5. Discussion

5.1. Comparison of the two approaches

From Fig. 8 we saw that the two analyses of the L1MI group gives comparable results with non-systematic deviations between 0 and 10%. The analysis based on laminate beam theory depends on a number of variables which can not be determined with great accuracy, such as the Young's moduli and thickness of individual layers. The curvature approach, on the other hand, depends on variables which can be determined with high accuracy, such as strains, moments and laminate beam thickness. It is therefore reasonable to assume that the curvature approach is the more accurate approach.

From Fig. 9 it is seen that the L1MM group has steady-state J values, J_{ss}, about 1650 J/m^2, while the laminate theory approach treatment of the L2MM group gives J_{ss} values around 1500 J/m^2 and the curvature approach treatment gives J_{ss} values around 3000 J/m^2. As mentioned above, it is expected that cracks along identical interfaces under identical moment combinations give similar J_{ss} values. The results in Fig. 9 therefore seem to indicate that the curvature approach based analysis of the L2MM group overestimates the J_{ss} values. However, from Fig. 7c-d it was observed that the L1MM group has two crack tips (and two fracture process zones), while the L2MM group has three crack tips. In effect, the cracks in the L2MM specimens create roughly 50% more new fracture surface area per unit length crack growth than cracks in the L1MM specimens. Therefore, as a first approximation, it is reasonable to expect that the specimens in the L2MM group have steady-state J values that are approximately 50% higher than the values for the specimens in the L1MM group. This hypothesis is largely consistent with the results in Fig. 9. Furthermore, this hypothesis is in agreement with the finding that the laminate theory approach underestimates the beam curvature, while the curvature approach is capable of determining the curvatures with low deviations. Hence it is reasonable to conclude that the laminate theory approach underestimates the J integrals for the L2MM group. It is not known why the laminate theory approach performs poorly for the L2MM group, considering that the two approaches are in good agreement for all other test groups.

It is an interesting finding, that by changing the ply thicknesses in the layup, one can change the cracking mechanism and thereby the steady-state fracture resistance of identical interfaces. The J_{ss} value for all single crack tip tests are around 750 J/m^2, while the two- and three crack tip tests have J_{ss} values around 1650 and 3000 J/m^2, respectively. It is an interesting idea that there might be an approximately linear dependency between the number of crack tips/fracture process zones and the steady state J values.

5.2. Crack growth initiation

From Table 3 it is seen that all specimens have comparable crack growth initiation energy values. The values are of the same order of magnitude as results from the literature for similar materials/interfaces systems [22]. When dividing the values into layup 1 and layup 2, the values are $359 \pm 55 J/m^2$ and $362 \pm 78 J/m^2$ respectively. Thus, no difference in crack initiation energy is seen between layup 1 and layup 2. This is not surprising since the conditions at the crack tip are identical for the two layups. For mode I and mixed mode, the crack growth initiation values are $314 \pm 49 J/m^2$ and $392 \pm 60 J/m^2$ respectively. Even though the difference between these results are not significant, there is a tendency that the mixed mode experiments have the highest crack initiation energies. It is reasonable to expect that there is a difference in the initiation energies, as the stress state at the crack tip is different for the two load configurations. For many interface systems, a higher amount of mode II results in a higher fracture energy [23].

5.3. Practical advantages and disadvantages of the curvature approach

For a homogenous DCB specimen consisting of a single material with well-known elastic properties, the laminate beam theory approach is rather straight-forward. However, when the examined DCB specimen consists of multilayer-beams, the laminate beam theory approach becomes more labour-intensive as the stiffness and thickness of all layers are required.

The curvature approach, on the other hand, is equally extensive for all types of DCB specimens. Performing the experiments using the curvature approach with the strain gauge measurement involves fixing strain gauges to the DCB beams and connecting (soldering) these to the strain gauge amplifier. This procedure takes some time. However, as layer thicknesses and stiffnesses are not required, it is not necessary to spend time determining these. Furthermore, not depending on values of layer thickness and stiffness implies that the curvature approach is likely to give more precise results than the laminate beam theory approach. The necessary inputs (moments and top and bottom beam strains) for the curvature approach can be determined with high accuracy, while the inputs for the laminate beam theory approach (lamina thicknesses and stiffnesses) are more difficult to determine. From the laminate beam theory expression in Eq. 15 it is seen that $J \propto E$ and $J \propto h^3$. This implies than measurement errors in lamina thickness are more critical than measurement errors in the lamina stiffness.

As mentioned in Section 2.2, when characterising a DCB specimen with symmetric beams it is only necessary to use one strain gauge per beam. Eventhough the beams in the present test were consided to be symmetric, two strain gauges were used per beam, in order to validate the above claim. Indeed, it was found that the readings from all strain gauge pairs had agreements within 2.5%, with an average value of 1.3%. Thus, with symmetric beams, it would be most convinient to place one strain gauge at the outside surface of each beam, thereby avoiding having to place strain gauges in the gap between the beams. The curvature approach is thus not only limited to adhesive joint testing but can also be used for delamination of laminates having symmetric beams. For a delamination test with unsymmetric beams it might be difficult to place find space for all necessary strain gauges. Furthermore, the agreements within strain gauge pairs justifies the decision to ignore the adhesive layer in the data analyses in Section 3.3.

An alternative to using strain gauges would be to use a digital image correlation system such as Aramis from Trilion Quality Systems [24] for the curvature measurements. Thereby time could be saved in specimen preparation, but the data analysis would probably be more extensive and time consuming.

As such, it is argued that the curvature approach is suitable for complex layups, where it has a number of advantages over the laminate theory approach. Furthermore, the curvature approach can be used for characterization of materials and assemblies with unknown parameters, such as test specimens cut from older constructions.

Finally, although it was not the scope of the present work, the mode I cohesive laws can be determined from the measured data on the J integral and the end-opening δ^* by fitting a suitable funtion to the J, δ^*-data and differenting the function [25].

6. Conclusions

An approach for determining the J integral for multilayer Double Cantilever Beams with Uneven Bending Moments (DCB-UBM) has been developed. This approach is based on the idea that the J integral can be found from beam curvatures and moments alone. The approach is especially well-suited for multilayer laminates, since no knowledge is needed on the thickness and Young's modulus of individual plies in the beams. This gives two advantages: The curvature approach is comfortable to use, as the equations and data treatment routines are much less extensive than the ones needed when applying the traditional laminate theory approach. The curvature approach is very accurate as the parameters on which it depends can be determined with great accuracy.

In the present work, the beam curvatures were determined by the use of strain gauges. The test specimens included two different layups subjected to two different load situation, such that four groups of experiments were conducted. Three of these showed excellent agreement between the curvature approach and the laminate theory approach, while it was found that the laminate theory approach underestimated the J integral massively for the fourth group.

Acknowledgments

The authors wish to thank LM Wind Power A/S (in particular Rune Vestergaard for donating test materials and Christian Lundsgaard-Larsen for kindly providing the Matlab code used for the laminate

approach). We also thank Christian H. Madsen for assistance with specimen preparation and Erik Vogeley for assistance with specimen testing. The DCB experiments leading to the results in this paper was conducted as part of a master project by Morten Rask. The research leading to these results has received funding from the European Comunity's Seventh Framework Programme (FP7/2007-2013) under grant agreement no 214467 (NATEX).

References

[1] Sørensen BF, Holmes JW, Brønsted P, Branner K. Blade Materials, testing methods and structural design, in Wind Power Generation and Wind Turbine Design (ed. Tong W). Southampton: WIT Press; pp. 417-465. 2010.
[2] Kafkalidis MS, Thouless MD. The effect of geometry and material properties of the fracture of single lap-shear joints. Int J Solids Struct 2002;39:4367-83.
[3] Yang QD, Thouless MD, Ward SM. Numerical simulations of adhesively-bonded beams failing with extensive plastic deformation. J Mech Phys Solids 1999;47:1337-53.
[4] Yang QD, Thouless MD. Mixed-mode fracture analysis of plastically-deforming adhesive joints. Int J Fract 2001;110:175-87.
[5] Li VC, Ward RJ. A novel testing technique for post-peak tensile behaviour of cementitious materials. Fracture toughness and fracture energy - testing methods for concrete and rocks (eds. Mihashi H, Takahashi H and Wittmann FH). Rotterdam: A. A. Balkema Publishers; pp. 183-95. 1989.
[6] Olsson P, Stigh U. On the determination of the constitutive properties of thin interphase layers - an exact inverse solution. Int J Fract 1989;41:R71-6.
[7] Suo Z, Bao G, Fan B. Delamination R-curve phenomena due to damage. J Mech Phys Solids 1992;40:1-16.
[8] Sørensen BF, Kirkegaard P. Determination of mixed mode cohesive laws. Eng Fract Mech 2006;73:2642-61.
[9] Sørensen BF, Jacobsen TK. Delamination of fibre composites: determination of mixed mode cohesive laws. Compos Sci Tech 2009;69:445-56.
[10] Bao G, Suo Z. Remarks on crack-bridging concepts. Appl Mech Rev 1992;45:355-61.
[11] Paris AJ, Paris PC. Instantaneous evaluation of J and C^*. Int J Fract 1988;8:R19-R21.
[12] Stigh U, Andersson T. An experimental method to determine the complete stress-elongation relationship for a structural adhesive layer loaded in peel, in Fracture of Polymers, Composites and Adhesives (eds. Williams JG and Pavan A). Amsterdam: ESIS Publication 27, Elsevier Science Ltd; pp. 297-306. 2000.
[13] Högberg JL, Sørensen BF, Stigh U. Constitutive behaviour of mixed mode loaded adhesive layer. Int J Solids Struct 2007;44:8335-54.
[14] O'Brian TK, Raju IS, Garber DP. Residual thermal and moisture influences on the strain energy release rate analysis of edge delamination. J Compos Tech Res 1986;8:37-47.
[15] Ozdil F, Carlsson LA. Characterisation of mixed mode delamination growth in glass/epoxy composite cylinders. J Compos Mater 2000;33:420-41.
[16] Lundsgaard-Larsen C, Sørensen BF, Berggreen C, Østergaard RC. A modified DCB sandwich specimen for measuring mixed-mode cohesive laws. Eng Fract Mech 2008; 75: 2514-30.´
[17] Sørensen BF, Jørgensen K, Jacobsen TK, Østergaard RC. DCB-specimen loaded with uneven bending moments. Int J Fract 2006;141:159-72.
[18] Rice JR. Mathematical analysis in the mechanics of fracture. Fracture, an advanced treatise, Vol. II (ed. H. Liebowitz). New York: Academic Press; 191-311. 1968.
[19] Rice JR. A path independent integral and the approximate analysis of stain concentration by notches and cracks. J Appl Mech 1968;35:379-86.
[20] Bao G, Ho S, Suo Z, Fan B. The role of material orthotropy in fracture specimens for composites. Int J Solids Struct 1992;29:1105-16.
[21] Albertsen H, Ivens J, Peters P, Wevers M, Verpost I. Interlaminar fracture toughness of CFRP influenced by fibre surface treatment: Part 1. Experimental results. Compos Sci Technol 1995;54:133-145.
[22] Sørensen BF, Goutianos S, Jacobsen TK. Strength scaling of adhesive joints in polymer–matrix composites. Int J Solids Struct 2009;46:741-61.
[23] Hutchinson JW, Suo Z. Mixed mode cracking in layered materials. Adv Appl Mech 1992;29:63–191.
[24] http://www.trilion.com/
[25] Sørensen BF, Jacobsen TK. Determination of cohesive laws by the J integral approach. Eng Fract Mech 2003;70:1841-58.